Progress In Electromagnetics Research Letters, Vol. 35, 37–49, 2012

ACTIVE WDM FILTER ON DILUTE NITRIDE QUANTUM WELL PHOTONIC BAND GAP WAVEGUIDE

G. Calò[1], D. Alexandropoulos[2], and V. Petruzzelli[1, *]

[1]Dipartimento di Elettrotecnica ed Elettronica, Politecnico di Bari, Via Re David n. 200, Bari 70125, Italy

[2]Department of Materials Science, University of Patras, Patras 26504, Greece

Abstract—A defective Photonic Band Gap device based on dilute nitrides is proposed as a high performance active wavelength filter for wavelength division multiplexing applications. The analyzed structure is made of GaInNAs-GaInAs multi quantum well ridge waveguides in which a geometrical defect in the periodic lattice induces selective transmission spectral regions centered at different wavelengths inside the photonic band gap. The multi-channel filter performances are evaluated as a function of both the defect length and the injected current value. The analysis is performed by using proprietary codes, based on the Bidirectional Beam Propagation Method with the Method of Lines introducing the rate equations. Highly selective 11-channel active filter with minimum value of the bandwidth at half-height $\Delta\lambda = 0.105\,\text{nm}$ with gain $G = 16.51\,\text{dB}$ has been assessed.

1. INTRODUCTION

Nowadays, the wavelength division multiplexing (WDM) demonstrates to be an indispensable technology to satisfy the increasing demand for expanding optical-fibre communication capacities. Light sources for WDM is required to have wide wavelength tunability, small chirping, and high temperature stability, whereas very high selective filters are needed for the dense WDM [1, 2].

In recent years, the Photonic Crystals (PCs) have offered novel possibilities for controlling the propagation and emission properties of light in integrated optical devices [3]. As the periodic potential in a crystal structure affects the electron motion, by defining allowed and

Received 24 July 2012, Accepted 24 August 2012, Scheduled 20 September 2012

* Corresponding author: Vincenzo Petruzzelli (petruzzelli@poliba.it).

forbidden electronic energy bands, in the same way, as an example, the periodic lattice of holes etched into a semiconductor material produces a band structure with a photonic band gap (PBG), where the propagation of light is forbidden. PCs can be used to create faster, smaller and more efficient optical devices for photonic communication networks and optical computing [4–6]. Moreover, thanks to their scaling property forbidden frequency bands can be obtained even in the microwave range by suitably scaling the geometric and/or the physical characteristics of the PBG structure [7].

More recently, a number of prototypal active devices, based on photonic crystals, were designed [8], constructed [9, 10] and tested [11] even for non-conventional microstructured optical fibers [12, 13].

In this paper, we design a multi-wavelength WDM filter based on GaInNAs-GaInAs Multi Quantum Wells (MQW) active ridge waveguides, patterned with a periodic one-dimensional grating and a defective region placed in the central layer. The presence of a defect of suitable length introduces localized states in the band gap and consequent transmission channels useful for the WDM filter [14]. In addition, dilute nitride GaInNAs compounds have received growing interest in the last decade, due to their potentiality for active device applications at the operating wavelength $\lambda = 1.3\,\mu\text{m}$. Moreover, the large conduction band offset induced by the introduction of Nitrogen in the InGaAs matrix leads to an efficient electron confinement in the quantum well (QW). Dilute nitrides proved advantageous in different applications such as laser transmitters, Semiconductor Optical Amplifiers (SOA) in optical communication systems and optical active switches [15, 16].

2. DESIGN OF THE ACTIVE WDM FILTER

The proposed active WDM filter is shown in Fig. 1. It is made of GaInNAs-GaInAs MQW ridge waveguides. It is evident that the periodic change of the ridge height creates a one-dimensional photonic crystal along the z propagation direction thus yielding a photonic band gap in the transmission spectrum. Moreover, in the central layer of the periodic lattice we have included a geometrical defect of length L_z, thus inducing a selective transmission of discrete wavelengths in the PBG. The geometrical parameters of the filtering periodic waveguiding structure have been chosen in order to obtain, for the corresponding device without defect, a PBG centred around the Bragg wavelength $\lambda_B = 1.2894\,\mu\text{m}$. With this aim, the examined structure is characterized by the following physical and geometrical parameters: ridge core of thickness $d_c = 0.103\,\mu\text{m}$, made of four

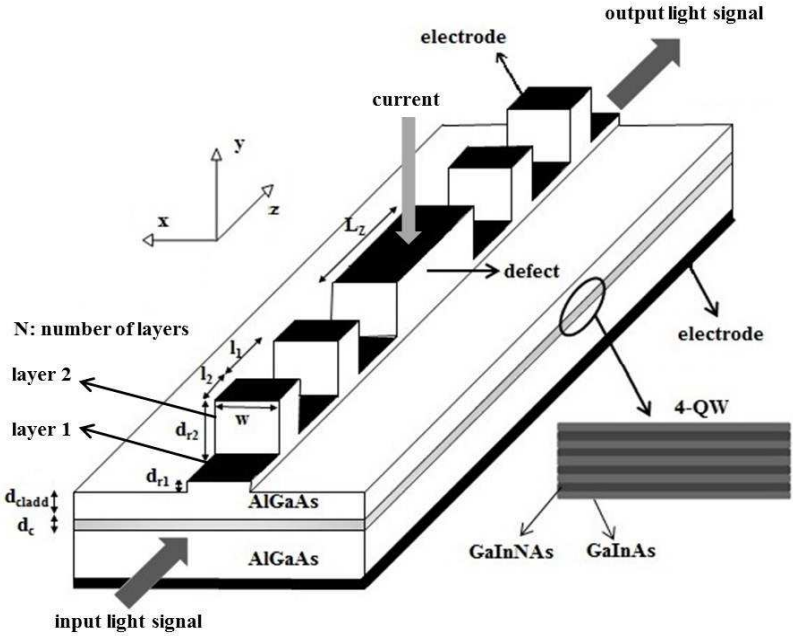

Figure 1. Layout of the active 1-D periodic waveguiding structure with defective region.

$Ga_{0.77}In_{0.23}N_{0.03}As_{0.97}$ quantum wells (QW) with refractive index $n_{\mathrm{GaInNAs}} = 3.65$ and thickness $d_{\mathrm{GaInNAs}} = 7\,\mathrm{nm}$, with $Ga_{0.8}In_{0.2}As$ barrier layers having refractive index $n_{\mathrm{GaInAs}} = 3.47$ and thickness $d_{\mathrm{GaInAs}} = 16.5\,\mathrm{nm}$; cladding layer with refractive index $n_{cladd} = 3.285$ and thickness $d_{cladd} = 0.220\,\mu\mathrm{m}$, ridge width $w = 2\,\mu\mathrm{m}$; substrate with refractive index $n_{sub} = 3.285$; number of alternating ridge waveguide layers $N = 1203$; grating unit cell with ridge heights $d_{r1} = 0.1\,\mu\mathrm{m}$ and $d_{r2} = 1.0\,\mu\mathrm{m}$ and lengths $l_1 = 0.120\,\mu\mathrm{m}$ and $l_2 = 0.076\,\mu\mathrm{m}$ of the first and the second layers, respectively. Electrodes have been considered along all the structure onto the ridge and down the AlGaAs substrate.

To evaluate the filtering performance of the defective periodic structure we have used for the electromagnetic (EM) propagation analysis a proprietary computer code based on the Bidirectional Beam Propagation Method with the Method of Lines (MoL-BBPM) [17]. It is a robust technique for the photonic device modelling, able to analyze the EM propagation step by step and to include further effects, e.g., the reflection effect at the discontinuities, the optical nonlinear effects, the electrooptical effect, and so on, applied along

the structure. In particular, the behaviour of the examined structure is deeply affected by the interaction of the injected current with the active materials acting along the whole structure. This effect is accounted by introducing in the computer code the following rate equations in the stationary analysis [18, 19]:

$$D_e \nabla^2 \sigma(x,y,z) = -\frac{J(z)}{e\, d_a} + \frac{g(x,y,z)}{e\, h\, v} \Gamma |E\,(x,y,z)|^2 + A\sigma + B\sigma^2 + C\sigma^3 \quad (1)$$

where $\sigma(x,\ y,\ z)$ is the charge density distribution, d_a the active layer thickness, $|E(x,y,z)|$ the electric field modulus, h the Planck constant, e the electron charge, J the injected current density, and $\Gamma = 0.044$ the optical confinement factor. The product hv is the photon energy expressed in eV. Moreover, $A = 2 \cdot 10^8\,\mathrm{s}^{-1}$, $B = 7 \cdot 10^{-17}\,\mathrm{m}^3\mathrm{s}^{-1}$, and $C = 4 \cdot 10^{-41}\,\mathrm{m}^6\mathrm{s}^{-1}$ are the non-radiative, the radiative, and the Auger recombination coefficients, respectively, $D_e = 0.001\,\mathrm{m}^2\mathrm{s}^{-1}$ is the diffusion coefficient, and $g(x,y,z)$ is the material gain, which describes the intrinsic property of a gain material [15].

The material gain $g(x,y,z)$ is obtained from the calculation of the electronic structure of GaInNAs based QWs. This was performed in the context of the Band Anticrossing Model to account for the N-induced nonparabolicity of the conduction band, and the 6×6 Luttinger-Kohn (LK) Hamiltonian for the valence bands accounting for the valence band mixing and the strain effects [15]. The electronic bandstructure is used in Fermi's Golden rule (free carrier theory) to yield material gain [15]. In this way the bandstructure effects are taken into account rigorously in the electromagnetic simulations.

The electric field $E(x,y,z)$, propagating along the waveguiding device is given from the solution of the wave equation:

$$\nabla^2 E\,(x,y,z) + k_0 n^2\,(x,y,z)\, E\,(x,y,z) = 0 \quad (2)$$

where k_0 is the vacuum wavenumber and $n(x,y,z)$ the complex refractive index. In the active medium, the complex refractive index $n_a(x,y,z)$ was calculated as [18, 19]:

$$n_a\,(x,y,z) = n_p + \beta_e\, \sigma\,(x,y,z) + j\frac{g\,(x,y,z)}{2k_0} \quad (3)$$

where n_p is the refractive index of the active medium when the charge injection is absent, and $\beta_e = -1.8{\cdot}10^{-26}\,\mathrm{m}^3$ is the anti-guide coefficient.

The theoretical expression of the material gain function $g(x,y,z,\lambda)$ has been approximated in our computer code by the following expression:

$$g\,(x,y,z,\lambda) = a_2\,(\lambda)\,\sigma^2\,(x,y,z,\lambda) + a_1\,(\lambda)\,\sigma\,(x,y,z,\lambda) + a_0\,(\lambda)\,. \quad (4)$$

where the coefficients a_2, a_1, and a_0 are determined at each wavelength value to achieve the best fitting of the material gain.

3. INFLUENCE OF THE DEFECT INCLUSION

The periodic structure without defect, i.e., $L_z = 0.076\,\mu\text{m}$, was first analysed in the passive case (i.e., injected current $I = 0\,\text{mA}$). We considered a simplified model of the passive case in which only the electromagnetic propagation is taken into account, whereas the rate equations and the losses are neglected. The Bragg wavelength occurs for $\lambda_B \cong 1.2894\,\mu\text{m}$, for which the maximum reflectance is $R_{\max} = 0.79$, whereas the minimum transmittance is $T_{\min} = 0.21$. Moreover, the band edges are equal to $\lambda_l = 1.2869\,\mu\text{m}$ and $\lambda_r = 1.2911\,\mu\text{m}$ thus achieving a band gap $B = 0.0042\,\mu\text{m}$.

The introduction of a defect, i.e., the central layer having different length L_z, modifies the transmittance spectrum and, by increasing the length of the defect L_z, transmission channels can be achieved in the PBG. Fig. 2 reports the transmittance spectra for different values of the defect length in the passive case: $L_z = 20\,\mu\text{m}$ (dashed curve), $L_z = 100\,\mu\text{m}$ (dotted curve), $L_z = 400\,\mu\text{m}$ (solid curve). We use a 3 dB definition to establish the number of the transmittance channels N_{ch} for the WDM applications. In fact, we assume that for each channel, having transmittance peak $T_{\max}$. the two adjacent transmittance minimum values must be lower than $T_{\max}/2$. By applying this definition, we can see that in the passive case for a defect length $L_z = 20\,\mu\text{m}$ no channel appears, while for $L_z = 100\,\mu\text{m}$ $\text{N}_{ch} = 1$, and for $L_z = 400\,\mu\text{m}$ $\text{N}_{ch} = 6$.

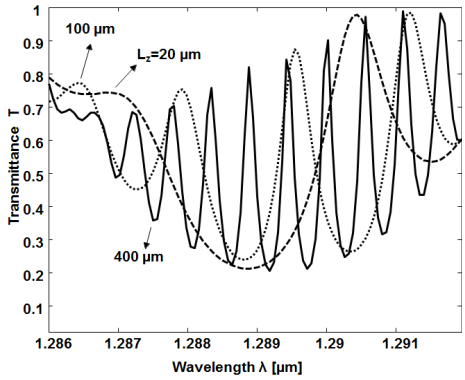

Figure 2. Transmittance T spectra of the examined periodic structure in the passive case (no injected current) and with defect lengths $L_z = 20\,\mu\text{m}$ (dashed curve), $L_z = 100\,\mu\text{m}$ (dotted curve), $L_z = 400\,\mu\text{m}$ (solid curve) by varying the defect length, transmission channels occur in the PBG.

Aiming at the design of multi-wavelength filters, we focus the analysis on defects having length $L_z \gg l_2$. In fact, as Fig. 2 shows, the number of transmission channels, corresponding to the localized states in the PBG, increases with the defect length. In particular, we verified that, in the passive case, no channel occurs up to defect lengths equal to $L_z = 50\,\mu\text{m}$. By increasing the defect length, the number of channels increases. As a further example, four channels are localized in the PBG when $L_z = 250\,\mu\text{m}$, whereas the channels become eight when $L_z = 500\,\mu\text{m}$.

Further changes in the transmittance spectrum occur by injecting current in the active dilute nitride region along all the grating and the defective structure having overall length $L_{tot} = (117.84 + L_z)\,\mu\text{m}$. In the active cases, we considered the complete numerical model in which both the electromagnetic propagation and the rate equation are taken into account.

As an example, Fig. 3 reports the transmittance spectra of the examined structure having defect length $L_z = 20\,\mu\text{m}$ and different values of the injected current ranging from $I = 12\,\text{mA}$ to $I = 22\,\text{mA}$, calculated by the complete model. For comparison, Fig. 3 shows the transmittance spectrum pertaining to the passive case, i.e., $I = 0\,\text{mA}$, (dashed curve) calculated by the simplified numerical model. In the presence of gain and absorption (i.e., in the active cases), the refractive

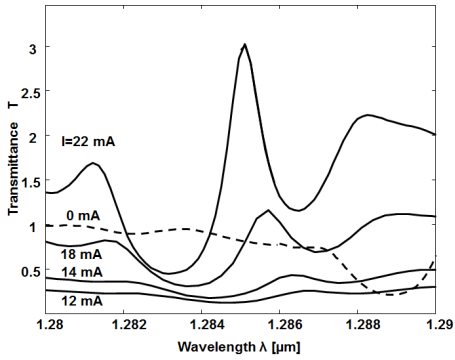

Figure 3. Transmittance T spectrum of the periodic structure with defect length $L_z = 20\,\mu\text{m}$ for 4 different values of the injected current: $I = 12\,\text{mA}$, $I = 14\,\text{mA}$, $I = 18\,\text{mA}$ and $I = 22\,\text{mA}$ (solid curves) and in the passive case $I = 0\,\text{mA}$ (dashed curve) In the passive case losses are neglected whereas in the active cases, when gain and absorption are considered, the refractive index of the examined active structure becomes a complex value, thus inducing a shift of the PBG.

index of the examined active structure becomes a complex value, thus contributing to the shift of the PBG as we can see from Fig. 3. Moreover, for the active structure, even for very low current values $I \cong 0\,\text{mA}$, being the absorption much greater than the material gain, the refractive index remains complex, thus giving a different transmittance spectrum behavior with respect to that calculated for the passive structure, for which the optical losses were neglected and the refractive index assumes always a real value. From Fig. 3, we can see that the band gap shifts towards lower wavelength values as the injected current increases from 12 mA to 22 mA and the transmittance peak shifts from $\lambda_r = 1.2870\,\mu\text{m}$ for $I = 12\,\text{mA}$ to $\lambda_r = 1.2850\,\mu\text{m}$ for $I = 22\,\text{mA}$, whereas the corresponding transmittance values increase from $T_r = 0.25$ (i.e., absorption is the dominant mechanism) to $T_r = 3.2$ (i.e., gain is the dominant mechanism), respectively, thus determining the formation of an active transmission channel absent when low current is injected. In fact, defining the transmittance gain as:

$$G = 10 \log_{10} (T_{\max})$$

where $T_{\max}$ is the maximum transmittance, we can assist to the formation of a transmission channel for $I = 22\,\text{mA}$ having a peak gain $G = 5\,\text{dB}$. Even though for $I = 18\,\text{mA}$ we have a peak gain $G > 0\,\text{dB}$ no channel appears.

4. DESIGN OF THE ACTIVE MULTICHANNEL WDM FILTER

To design active multichannel WDM filters we must use longer defects. In fact, by inspection of Fig. 2 we have verified that by changing the defect length values from $L_z = 20\,\mu\text{m}$ to $L_z = 400\,\mu\text{m}$ the channel number increases from $N_{ch} = 0$ to $N_{ch} = 6$. Otherwise, by activating the quantum well ridge waveguiding structure the channel number increasingly grows and each channel is characterized by increasing gain values. This is due to the injected current and to the Eq. (3) that shows as the complex refractive index n_a in the active region changes versus the carrier density σ evaluated by the rate Eq. (1) in dependence of the injection current I.

The change of the real part of the refractive index contributes to the shift of the transmission channels in the PBG and their increasing number with I, whereas the imaginary part of n_a gives increasing gain values thus allowing that some peaks can be considered new channels.

To better clarify this mechanism of the increasing channel number, Fig. 4 shows the transmittance spectra of the structure having a defect length $L_z = 400\,\mu\text{m}$ for 6 increasing injected current values:

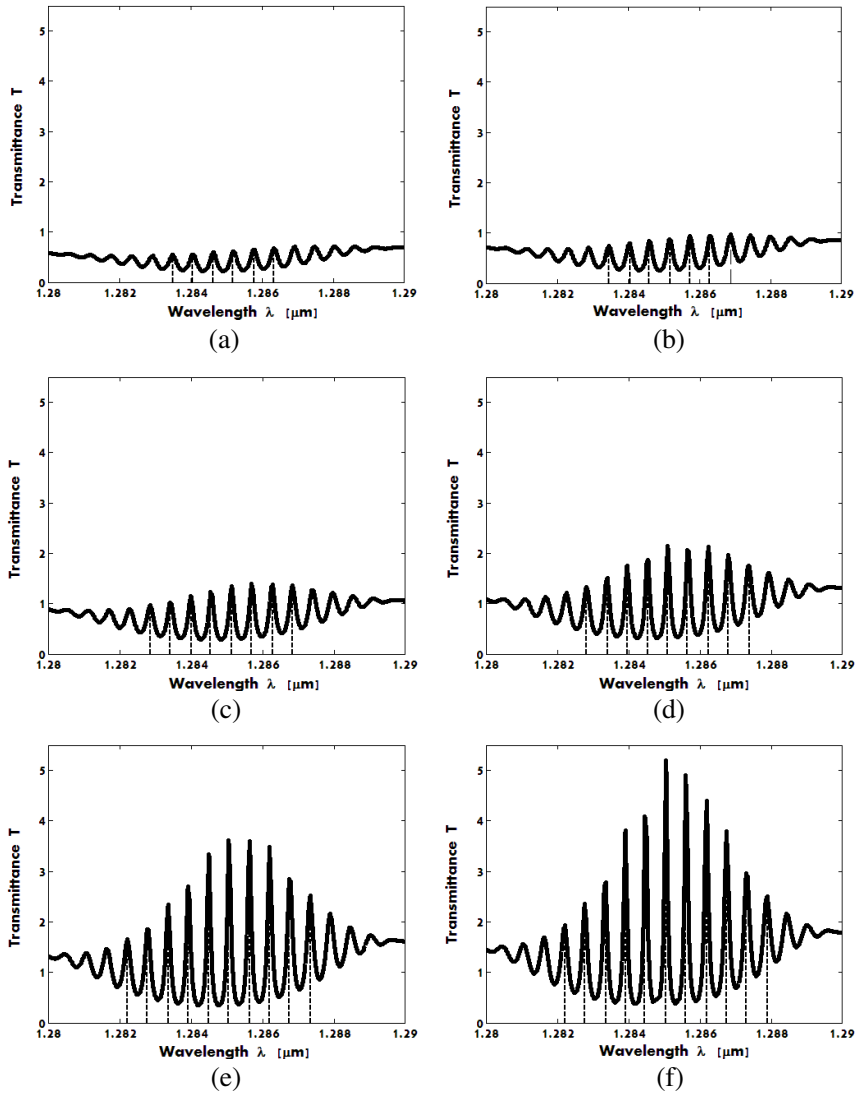

Figure 4. Transmittance spectra of the active periodic structure for defect length $L_z = 400\,\mu\text{m}$ and different values of the injected current: (a) $I = 62\,\text{mA}$, (b) $I = 63\,\text{mA}$, (c) $I = 64\,\text{mA}$, (d) $I = 65\,\text{mA}$, (e) $I = 66\,\text{mA}$, (f) $I = 66.5\,\text{mA}$. By changing the injected current from $I = 62\,\text{mA}$ to $I = 66.5\,\text{mA}$ the channel number increases from 6 to 11.

(a) $I = 62\,\text{mA}$, (b) $I = 63\,\text{mA}$, (c) $I = 64\,\text{mA}$, (d) $I = 65\,\text{mA}$, (e) $I = 66\,\text{mA}$, and (f) $I = 66.5\,\text{mA}$. We can see that for increasing I values the channel number increases from $N_{ch} = 6$ to $N_{ch} = 11$. Fig. 5 reports the central λ_0 wavelength values of the transmission channels for different I values ranging from $I = 62$ to $I = 66.5\,\text{mA}$. As an example, for $I = 62\,\text{mA}$ 6 channels are activated, while for $I = 63\,\text{mA}$, besides the previous 6 channels CH3–CH8, the channel CH9 appears. Moreover, for $I = 64\,\text{mA}$ the channel CH2 adds to the others 7. At last, for $I = 66.5\,\text{mA}$ all the 11 channels are active. We can see that for each CH channel the central wavelengths λ_0 slightly shift by changing I from 62 mA to 66.5 mA. As an example, for the channel CH6 the λ_0 value changes from 1.28518 μm to 1.28504 μm for I increasing from 62 mA to 66.5 mA.

Figure 6 shows the gain G [dB] calculated in correspondence of the central wavelength for the activated channels CH1–CH11 for the different I values. We can observe that for $I = 62\,\text{mA}$ the activated channels CH3–CH8 assume negative gain values (i.e., the gain g of Eq. (4) does not compensate the optical losses). Otherwise, by increasing the injected current to $I = 64\,\text{mA}$ all the channels assume positive gain value with the exception of the channel CH2, having $G = -0.30\,\text{dB}$.

Further increasing the current for $I \geq 65\,\text{mA}$ all the activated channels assumes positive gain G values and the maximum gain occurs for the channel CH6, that for $I = 66.5\,\text{mA}$ assumes a gain value $G = 16.51\,\text{dB}$.

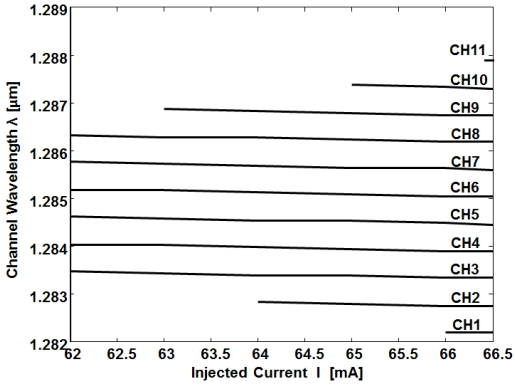

Figure 5. Central λ_0 wavelength values of the transmission channels from CH1 to CH11 as a function of the injected current I for defect length $L_z = 400\,\mu\text{m}$.

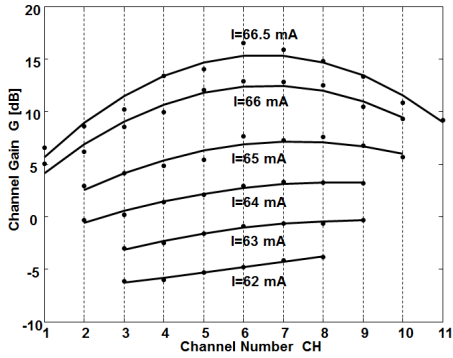

Figure 6. Gain G [dB] calculated in correspondence of the central wavelength for the activated channels CH1–CH11 for the different I values and defect length $L_z = 400\,\mu\text{m}$.

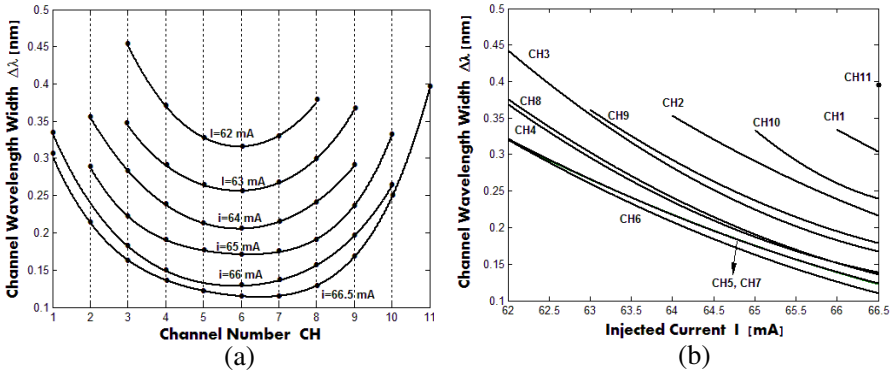

Figure 7. (a) Channel wavelength width $\Delta\lambda$ for the different WDM channels CH1–CH11 and for injected currents $I = 62\,\text{mA}$, $I = 63\,\text{mA}$, $I = 64\,\text{mA}$, $I = 65\,\text{mA}$, $I = 66\,\text{mA}$, and $I = 66.5\,\text{mA}$ for defect length $L_z = 400\,\mu\text{m}$. (b) Channel wavelength width $\Delta\lambda$ as a function of the injected current I and for the activated WDM channels for defect length $L_z = 400\,\mu\text{m}$.

In Fig. 7, the calculated channel wavelength width $\Delta\lambda$ values are plotted as a function of both the channel CH (a) and the injected current I (b).

By the inspection of Fig. 7(a), we can see that for all the activated channels lower bandwidth $\Delta\lambda$ values occur for higher injected current values. As an example, for the channel CH6 $\Delta\lambda$ decreases from 0.318 nm for $I = 62\,\text{mA}$ to 0.105 nm for $I = 66.5\,\text{mA}$. On the other

hand, from Fig. 7(b) we can verify that for the channels CH5 and CH7 the curves of $\Delta\lambda$ as a function of the injected values are coincident, whereas the channels CH4 approaches almost the same bandwidth $\Delta\lambda$ values of those of CH8. Even the channels CH3 and CH9 assume almost the same bandwidth $\Delta\lambda$ values for $I \geq 63\,\text{mA}$. The best WDM performances are evident for the channel CH6 that assumes higher gain values and lower bandwidth $\Delta\lambda$ values for each I value. In particular, for $I = 66.5\,\text{mA}$ the channel CH6 shows wavelength $\Delta\lambda = 0.105\,\text{nm}$ with gain $G = 16.51\,\text{dB}$.

5. CONCLUSIONS

The performances of a wavelength filtering active device based on a dilute nitrides multi-quantum-well PBG structure have been investigated. The interaction of the injected current with the active quantum-well waveguide has been accounted by the rate-equation, while the optical propagation characteristics of the periodic structure have been carried out by means of proprietary computing codes based on the MoL-BBPM. The influence of the inclusion of a defect in the central layer on the transmittance and reflectance spectra has been evaluated. Transmission channels appear in the band gap by increasing the defect length up to 100 µm. In particular, 6 transmission channels occurs for a defect length of 400 µm. On the other hand, 11-wavelength selective channels with maximum gain $G = 16.51\,\text{dB}$ and minimum bandwidth $\Delta\lambda = 0.105\,\text{nm}$ have been obtained with a defect length $L_z = 400\,\mu\text{m}$ and injected current $I = 66.5\,\text{mA}$.

ACKNOWLEDGMENT

The research has been conducted in the framework of the European Cooperation in Science and Technology ("COST") Action MP0805 and has been supported by the Photonic Interconnect Technology for Chip Multiprocessing Architectures ("PHOTONICA") project under the Fondo per gli Investimenti della Ricerca di Base 2008 ("FIRB") program, funded by the Italian government and by the project "Regional laboratory for synthesis and characterization of new organic and nanostructured materials for electronics, photonics, and advanced technologies" funded by the Apulia Region.

REFERENCES

1. Kumar, A., B. Suthar, V. Kumar, K. S. Singh, and A. Bhargava, "Tunable wavelength demultiplexer for DWDM application using

1-D photonic crystal," *Progress In Electromagnetics Research Letters*, Vol. 33, 27–35, 2012.

2. Wu, C.-J., M.-H. Lee, W.-H. Chen, and T.-J. Yang, "A mid-infrared multichanneled filter in a photonic crystal heterostructure containing negative-permittivity materials," *Journal of Electromagnetic Waves and Applications*, Vol. 25, No. 10, 1360–1371, 2011.
3. Grande, M., G. Calo, V. Petruzzelli, and A. D'Orazio, "High-Q photonic crystal nanobeam cavity based on a silicon nitride membrane incorporating fabrication imperfections and a low-index material layer," *Progress In Electromagnetics Research B*, Vol. 37, 191–204, 2012.
4. D'Orazio, A., M. De Sario, V. Marrocco, and V. Petruzzelli, "Photonic crystal drop filter exploiting resonant cavity configuration," *IEEE Transactions on Nanotechnology*, Vol. 7, No. 1, 10–13, 2008.
5. D'Orazio, A., M. De Sario, V. Ingravallo, V. Petruzzelli, and F. Prudenzano, "Infiltrated liquid crystal photonic bandgap devices for switching and tunable filtering," *Fiber and Integrated Optics*, Vol. 22, No. 3, 161–172, 2003.
6. Calò, G., A. Farinola, and V. Petruzzelli, "Equalization in photonic bandgap multiwavelength filters by the Newton binomial distribution," *Journal of the Optical Society of America B: Optical Physics*, Vol. 28, No. 7, 1668–1679, 2011.
7. D'Orazio, A., M. De Sario, V. Gadaleta, V. Petruzzelli, and F. Prudenzano, "Meander microstrip photonic bandgap filter using a Kaiser tapering window," *Electronics Letters*, Vol. 37, No. 19, 1165–1167, 2001.
8. Park, H. G., J. K. Hwang, J. Huh, H. Y. Ryu, S. H. Kim, J. S. Kim, and Y. H. Lee, "Characteristics of modified single-defect two-dimensional photonic crystal lasers," *IEEE J. Quantum Electron.*, Vol. 38, 1353–1365, 2002.
9. Stomeo, T., F. Prudenzano, M. D. Vittorio, V. Errico, A. Salhi, A. Passaseo, R. Cingolani, and V. Petruzzelli, "Design and fabrication of active and passive photonic crystal resonators," *Microelectronic Engineering*, Vol. 83, Nos. 4–9, 1823–1825, 2006.
10. Matsubara, H., S. Yoshimoto, H. Saito, Y. Jianglin, Y. Tanaka, and S. Noda, "GaN photonic-crystal surface-emitting laser at blue-violet wavelengths," *Science*, Vol. 319, 445–447, 2008.
11. Lee, P.-T., T.-W. Lu, and K.-U. Sio, "Multi-functional light emitter based on band-edge modes near Γ-point in honeycomb photonic crystal," *Journal of Lightwave Technology*, Vol. 29, No. 12, 1797–1801, 2011.

12. Carlone, G., A. D'Orazio, M. De Sario, L. Mescia, V. Petruzzelli, and F. Prudenzano, "Design of double-clad erbium-doped holey fiber amplifier," *Journal of Non-crystalline Solids*, Vol. 351, Nos. 21–23, 1840–1845, 2005.
13. Prudenzano, F., L. Mescia, A. D'Orazio, M. De Sario, V. Petruzzelli, A. Chiasera, and M. Ferrari, "Optimization and characterization of rare-earth-doped photonic-crystal-fiber amplifier using genetic algorithm," *Journal of Lightwave Technology*, Vol. 25, No. 8, 2135–2142, 2007.
14. Wang, Z.-Y., X.-M. Cheng, X.-Q. He, S.-L. Fan, and W.-Z. Yan, "Photonic crystal narrow filters with negative refractive index structural defects," *Progress In Electromagnetics Research*, Vol. 80, 421–430, 2008.
15. Alexandropoulos, D., M. J. Adams, Z. Hatzopoulos, and D. Syvridis, "Proposed scheme for polarization insensitive GaInNAs-based semiconductor optical amplifiers," *IEEE J. Quantum Electron.*, Vol. 41, 817–822, 2005.
16. Calò, G., D. Alexandropoulos, A. D'Orazio, and V. Petruzzelli, "Wavelength selective switching in dilute nitrides multi quantum well photonic band gap waveguides," *Physica Status Solidi (B) Basic Research*, Vol. 248, No. 5, 212–1215, 2011.
17. D'Orazio, A., M. De Sario, V. Petruzzelli, and F. Prudenzano, "Bidirectional beam propagation method based on the method of lines for the analysis of photonic band gap structures," *Opt. Quantum Electron.*, Vol. 35, 629–640, 2003.
18. Calò, G., A. D'Orazio, M. Grande, V. Marrocco, and V. Petruzzelli, "Active InGaAsP/InP photonic bandgap waveguides for wavelength-selective switching," *IEEE J. Quantum Electron.*, Vol. 47, No. 2, 172–181, 2011.
19. Calò, G., V. Petruzzelli, L. Mescia, and F. Prudenzano, "Study of gain in photonic band gap active InP waveguides," *Journal of the Optical Society of America B*, Vol. 26, 2414–2422, 2009.